Journal of Controlled Release 373 (2024) 533–546

Contents lists available at ScienceDirect

Journal of Controlled Release

journal homepage: www.elsevier.com/locate/jconrel

Impact of immediate release film coating on the disintegration process of tablets

Mingrui Ma [a], Daniel Powell [b,c], Marwa Nassar [d], Jason Teckoe [d], Daniel Markl [b,c], J. Axel Zeitler [a,*]

[a] Department of Chemical Engineering and Biotechnology, University of Cambridge, Philippa Fawcett Drive, Cambridge CB3 0AS, UK
[b] Centre for Continuous Manufacturing and Advanced Crystallisation, University of Strathclyde, Glasgow G1 1RD, UK
[c] Strathclyde Institute of Pharmacy and Biomedical Sciences, University of Strathclyde, Glasgow G4 0RE, UK
[d] Colorcon Ltd, Flagship House, Victory Way, Dartford DA2 6QD, UK

ARTICLE INFO

Keywords:
Tablet
Film coating
Terahertz pulsed imaging
Optical coherence tomography
Disintegration
Dissolution
Immediate release

ABSTRACT

Pharmaceutical tablets are often coated with a layer of polymeric material to protect the drug from environmental degradation, facilitate the packaging process, and enhance patient compliance. However, the detailed effects of such coating layers on drug release are not well understood. To investigate this, flat-faced pure microcrystalline cellulose tablets with a diameter of 13 mm and a thickness between 1.5 mm to 1.6 mm were directly compressed, and a film coating layer with a thickness of 80 μm to 120 μm was applied to one face of these tablets. This tablet geometry and immediate release film coating were chosen as a model system to understand how the film coating interacts with the tablet core. The coating hydration and dissolution process was studied using terahertz pulsed imaging, while optical coherence tomography was used to capture further details on the swelling process of the polymer in the coated tablet. The study investigated the film coating polymer dissolution process and found the gelling of dissolving polymer restricted the capillary liquid transport in the core. These findings can help predict the dissolution of film coating within the typical range of thickness (30 μm to 40 μm) and potentially be extended to understand modified release coating formulations.

1. Introduction

The pharmaceutical tablet is the most common solid oral dosage form to administer drug or active pharmaceutical ingredient (API) to patients [1,2]. Specifically, immediate release tablets are designed to release all API over a relatively short period to achieve rapid onset of drug effects and maximise the bioavailability of poorly soluble API [2]. However, some APIs are vulnerable to moisture or UV radiation-induced decomposition. Therefore, it is common to apply a film coating layer to protect the tablet core before administration, and the coating should dissolve as quickly as possible once the tablet enters the gastrointestinal (GI) tract [3]. There are also modified release coatings to delay or extend the release of the API into the GI tract [4,5]. The pH-dependent enteric coatings can be utilised to protect the API from the acidic environment in the stomach, while other polymer film coatings can play the role of the diffusion barrier to maintain the API release over a long period [5]. As a result, the coating thickness and its dissolution can directly impact the performance of the drug product. The disintegration and dissolution tests are standardised methods outlined in the pharmacopoeias to establish whether the dosage forms meet their quality standards. For decades, these compliance tests have been considered the most effective *in vitro* method to test the quality of solid dosage forms [2,6]. However, results from the said tests provide us with limited opportunity to further understand the mechanisms of tablet disintegration and dissolution, much less the process of film coating disintegration or dissolution in detail.

The immediate release film coating is often believed to cast negligible influences on the disintegration of tablets. However, the dissolution medium (*e.g.*, water) needs to permeate the said coating layer before the tablet core can become hydrated for film-coated tablets [7]. Water then hydrates and activates the disintegrant particles, which swell to initiate the tablet core disintegration [6]. The film coating, therefore, acts as a water transport barrier. The hydration and subsequent dissolution of the coating layer is a complex process. For example, swelling of the coating polymer can introduce inhomogeneity in the film coating to initiate the polymer dissolution [8]. The hydrated coating polymer then

* Corresponding author.
E-mail address: jaz22@cam.ac.uk (J.A. Zeitler).

https://doi.org/10.1016/j.jconrel.2024.07.037
Received 7 May 2024; Received in revised form 12 July 2024; Accepted 15 July 2024
Available online 27 July 2024

forms a layered structure with different thermodynamic states [9]. This layered structure is likely to reduce the transport of water to the tablet core, resulting in a slowdown of subsequent water penetration in the porous matrix of the core compared with uncoated tablets [3]. In contrast, if the tablet core beneath the film coating is hydrated at the same time, the swelling of the disintegrant in the core can produce stress at the core-coating boundary that triggers faster coating and tablet core disintegration [2]. The cascade of interactions and responses following water ingress are poorly understood in the literature. Hence, a detailed investigation of the liquid transport behaviour is critical to offer mechanistic information to design film-coated tablets effectively and to model their disintegration performance.

Several methods have been used to understand the mechanism of tablet disintegration processes, including volumetric apparatus [10], force-displacement apparatus [11–13], high-speed video imaging [14], magnetic resonance imaging (MRI) [15–17], UV imaging [18,19], among others. Although quantitative measurements of the water transport kinetics can be performed, these methods have primarily focussed on the disintegration of the tablet core and have yet to consider in detail the disintegration of film-coated tablets. Volumetric, force-displacement and video imaging measurements are well-established and straightforward methods to investigate the disintegration of tablets. However, researchers find the methods challenging to directly track the liquid front within the porous media. Further, UV imaging can only be utilised to characterise non-transparent liquids/solids, while MRI characterisation is too slow to start measurements for fast disintegration processes. Holographic interferometry and electronic speckle pattern interferometry are valuable techniques to study drug release by diffusion through a gel layer [20]. Furthermore, new techniques such as broadband acoustic resonance dissolution spectroscopy [21] and 3D tomographic laser-induced fluorescence imaging [22] are seen in the literature to provide more quantitative characterisations on the tablet disintegration process.

Terahertz Pulsed Imaging (TPI) has been applied to examine pharmaceutical dosage forms and study the depth-resolved features non-destructively in reflection [23]. The terahertz waveforms in the time domain provide information on the refractive indices of the sample studied [24,25]. This feature further enables us to extract the sample porosity [25] or to analyse the thickness of a thin sample, *e.g.*, the film coating thickness [5,23,26]. Since the wavelength of terahertz radiation is longer than the typical size of pharmaceutical particles (50 μm to 100 μm), broadband terahertz radiation can be utilised to explore features in tablets without much attenuation. The time-domain terahertz waveform contains depth-resolved information collected by the terahertz detector after a terahertz pulse is sent to a sample of interest. When the terahertz pulse arrives at an interface between two media in a porous sample, a reflection of the pulse will take place if the medium that the pulse is entering does not absorb all the energy of the pulse (Fig. 1). The Fresnel equations [8,27] can predict the proportion of the pulse reflected back to the detector:

$$r_{\text{measured}} = \left(\frac{n_{\text{medium1}} - n_{\text{medium2}}}{n_{\text{medium1}} + n_{\text{medium2}}}\right)^2 \quad (1)$$

where r_{measured} is the reflectivity whose square root ($\sqrt{r_{\text{measured}}}$) is proportional to the terahertz signal amplitude, n_{medium1} is the refractive index of the medium the terahertz pulse enters from and n_{medium2} is the refractive index of the medium the terahertz pulse enters into. Hence, if one continuously acquires the reflected pulses as water transports through a sample, the water penetration front in the sample can be tracked by investigating the reflection peak on the optical time delay line of the time-domain terahertz waveforms [28]. The underlying principle of TPI was employed to investigate the water transport kinetics in pharmaceutical tablets. The literature views TPI as a technique of low energy radiation, fast data acquisition, and calibration-free [25]. Hence, samples can be studied rapidly *in situ* in real-time without changing the sample integrity due to thermal warm-up by the radiation. Key challenges facing TPI include the drop in signal-to-noise with increasing

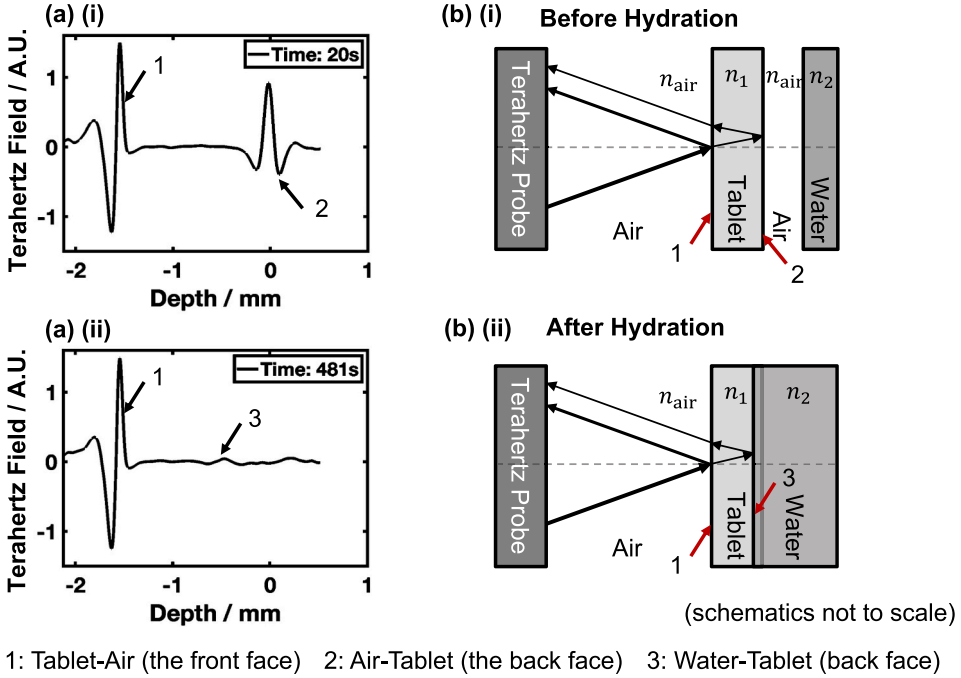

Fig. 1. Principle of terahertz pulsed imaging (TPI) with (a) the deconvoluted time-domain waveforms and (b) schematics illustrating the detection of terahertz pulses that reflected from interfaces before and after the hydration of the tablet. The time-domain waveforms acquired from the TPI illustrate the spatial information of the tablet interfaces. The sudden change of the effective refractive index at the interface leads to the reflection peaks on the waveforms. Reflection peaks from these interfaces are labelled on the waveforms. Tracking these peaks yields the depth-resolved information of the tablet disintegration process. Legends in (a) show the time after the TPI acquisition begins.

sample thickness and the strong attenuation of terahertz radiation by bulk water [29]. Yet, given that the measurements in film-coated tablets are sufficiently short-ranged to allow for sufficient signal-to-noise signal to propagate through the structures such that commercial terahertz spectrometers can be employed for the analysis, TPI is a versatile platform to study water transport directly through different film-coated tablets. Since the change in refractive index between the dry tablet core and water is sufficiently high, the water-tablet interface can be well characterised by TPI.

Optical coherence tomography (OCT) is another robust technique to study sub-surface structures, *e.g.* film-coated tablets [30]. Used conventionally as a medical imaging tool, OCT can be utilised as a pharmaceutical process analytical technology to monitor the coating process in-line or perform end-of-product tests on the coating thickness. OCT works by employing a large bandwidth (high spatial) and several microns coherence length (low temporal) light sources [30]. The technique can generate depth-resolved vision by performing 2-D or 3-D cross-sectional depth scans. The scans compare the time-of-flight between the single scattered photons and the reference beam. In applications, OCT can visualise the cross-sectional changes in refractive index at the boundary by performing scans that record both the coherent light absorption through A-scans and B-scans (Fig. 2), which are similar nomenclatures as those used in ultrasonic imaging. The A-scan is a single scan into the thickness of the film-coated tablet, while the B-scan combines a series of A-scan images along the radial direction of the tablet [31]. OCT has been explored for applications such as determining the thickness of the coating layer off-line [32] or in-line [30], monitoring the dissolution process of uncoated dosage forms [31], investigating the multilayer coatings [33] and studying the acid protection from enteric coatings [34]. Although the acquisition rate of the commercial OCT equipment (0.33 Hz) was set to a much slower rate than the acquisition rate of TPI (15 Hz), it is sufficiently fast to characterise the swelling of the film coating. It is important to note that the OCT acquisition rate can be orders of magnitude faster than TPI but that a tradeoff is made during acquisition between the signal-to-noise required, the dynamics of the process and the data storage needed for the experimental data. Attempts have been made previously to compare the coating thickness determined by TPI and OCT [17]. The complementary features of TPI and OCT in terms of resolution (OCT > TPI) and imaging depth (TPI > OCT) provide an excellent case to couple these techniques to improve the interpretation of the film-coated tablet disintegration process significantly [35,36].

We previously utilised TPI to mechanistically understand the liquid transport process through different placebo tablets at room temperature. Early studies focussed on using the power law model (Eq. 2) to investigate liquid transport kinetics and mass transport mechanism through uncoated tablets [8].

$$y = kt^m \tag{2}$$

where y is the liquid front position in the porous medium, m is the power law constant, which describes the mass transport mechanism, k is the pre-exponent constant, and t is the time after the liquid penetration starts. The m and k constants can be determined by taking natural logarithms on both sides of Eq. (2) and fitting experimental data extracted from TPI to the linear equation.

The power law constants m and k were found to correlate to the physical properties of the tablet and dissolution medium, such as liquid temperature, tablet porosity and tablet formulation [24]. The liquid transport behaves differently depending on whether the porous matrix can swell or not [27,28]. Follow-up studies began to characterise the disintegration process of coated tablets. The polyvinyl alcohol (PVA) based Opadry II coated microcrystalline cellulose (MCC) tablets were found to swell and form a gel in the coating layer once hydrated, and the water transport in the tablet core slowed down subsequently [3,6]. However, the swelling of the polymer in the coating and core cannot be sufficiently addressed with only TPI. Besides, the porous matrix's water transport rate slowed down after film coating with the PVA-based formulation. The mechanism that led to the slower waterfront penetration needs further characterisation.

This study will extend the scope to two different Opadry II formulations, a PVA-based formulation and a hydroxypropyl methylcellulose (HPMC) based immediate release film coating formulation, and systematically contrast the difference between their disintegration or dissolution process using TPI and OCT for the first time. For all formulations, we continue to use MCC tablet cores. Using a combination of different imaging techniques is necessary to map out the disintegration process of film-coated tablets more precisely. The flat-faced tablets were chosen due to their geometric simplicity (cylindrical), ease of manufacture, and potential to film coat the tablet uniformly. The overall results from this simple model will hopefully lay the foundation and offer preliminary insights on the predictive modelling for the disintegration process of film-coated tablets.

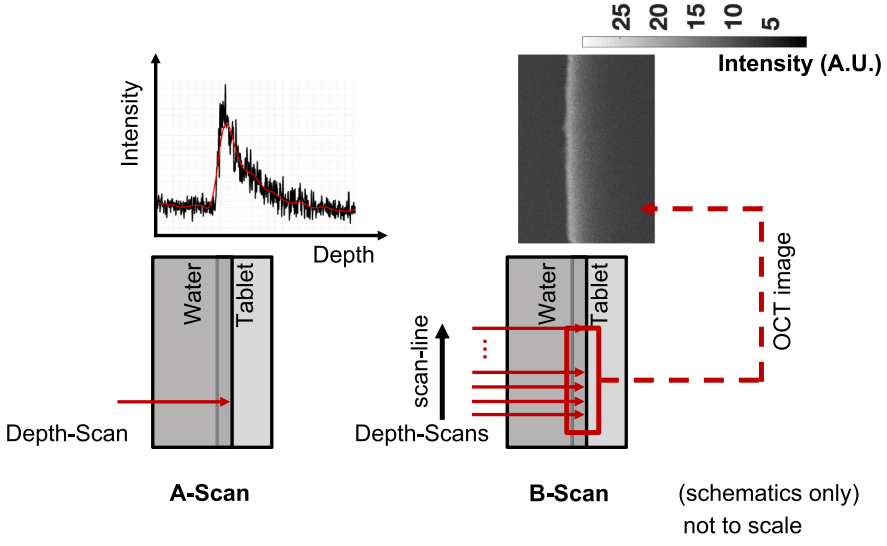

Fig. 2. OCT A-scan and B-scan in this study. The A-scan refers to the scan at a single depth only. The B-scan combines these single-depth scans at different points along the tablet surface to generate the 2-D image of the tablet cross-section.

2. Materials and methods

2.1. Tablet preparation

Tablet cores were prepared by direct compression of pure excipient powder. Microcrystalline cellulose (MCC, Avicel PH102) powder was directly compressed into 13 mm-diameter tablets using a compaction simulator (HB50, Huxley Bertram Engineering Ltd., Cambridge, UK) that mimicked the process of an industrial scale rotary compaction machine. An example of the compaction profile can be found in the appendix. The target thickness ranged from 1.5 mm to 1.6 mm, which can be adjusted by varying the gap width between the upper and the lower punch during the compaction. Maximum compaction forces of about 28 kN, 18 kN and 12 kN are required to reach the 10%, 15% and 20% target porosities to model the low, medium and high porosity tablet disintegration respectively. 18 MCC tablets were prepared at each compaction force. The tablet porosities were calculated using the relative density method [28]:

$$f = 1 - \rho_{\text{relative}} = 1 - \frac{\rho_{\text{bulk}}}{\rho_{\text{true}}} = 1 - \frac{4M}{\pi d^2 H \rho_{\text{true}}} \quad (3)$$

where d and H are the tablet diameter and thickness, respectively, measured using a micrometer (Sealey AK9635D.v3, Suffolk, UK), M is mass, and ρ is density. The true MCC density was quoted from the literature [37].

Measurements were carried out immediately after the compaction and 17 days after compaction to account for long-run mechanical relaxation. The tablets were sealed in polyethylene sample bags and stored under standard lab conditions between measurements.

We found an average 1.27% volume increase for the MCC tablets between the two measurements due to MCC swelling under ambient storage conditions and long-term elastic recovery.

2.2. Film coating

All tablets were coated 17 days after compaction to ensure complete mechanical stress relaxation. A custom-built research coating spray rig at Colorcon was used to apply the film coating layer [3]. Tablets were divided into two batches. In Batch 1, we chose 12 tablets from each of the three different porosities and coated with a PVA (Opadry II 85F18422, Colorcon, Dartford, UK) based on a complete coating formulation. The remaining 18 tablets in Batch 2 were film coated with an HPMC (Opadry II 47U180002, Colorcon, Dartford, UK) based complete coating formulation. Both formulations contain titanium dioxide. Tablets were adhered to a metal plate *via* blu-tack so that the top surfaces of the tablets were exposed to the spray. The coating operation commenced by switching on the coating spray nozzle. Suspensions with 10%wt Opadry II were reconstituted in deionised water for 45 min using a paddle-mixer at a 300 rpm stir rate. A peristaltic pump was then used to feed the suspension to the nozzle. The tablets first underwent two slow spray cycles (22 rpm pump feed rate), followed by about 10 fast spray cycles (63 rpm pump feed rate). Each cycle comprised a spray round (nozzle: on, dryer: off) and a drying round (nozzle: off, dryer: on). In the drying round, heated air was blown over the tablets' surface to evaporate the aqueous solution. All 54 tablets were successfully film-coated. The target coating thickness (80 μm 120 μm) was confirmed by measuring the thickness before and after coating using a micrometer (Sealey AK9635D.v3, Suffolk, UK). The changes in mass and thickness of the tablets due to the film coating are recorded in Table 1. In our previous studies, the TPI imaga system has been utilised to study the variation of film thickness along the tablet surface [38]. We have also used X-ray computed tomography to obtain a cross-sectional image of the tablet film coated following the same film coating protocol [3]. The film coating layer was found to be relatively uniform along the tablet face.

2.3. 3D-printed sample holder

A customised sample holder (Fig. 3) was 3-D printed from sintered nylon (Nylon 12, Formlabs, Boston, MA) using a Formlabs 3-D printer (Fuse 1+, Formlabs, Boston, MA). The film-coated tablets were then mounted in the cylindrical aperture of the sample holder. The gap between the edge of the aperture and the band of the tablet was sealed using epoxy resin that cured under UV light for about 20 s, so only the film-coated surface was exposed to the surroundings. This means that the band of the tablet, which is free of coating, will not be directly hydrated.

2.4. TPI measurement and data analysis

A commercial time-domain terahertz system was used to perform TPI measurements (TeraPulse 4000, TeraView Ltd., Cambridge, UK). All measurements were carried out at ambient temperatures (about 21°C). This temperature is chosen as a starting point as it can be relatively well-controlled under lab conditions to prevent any temperature variation from influencing the polymer dissolution rate. The sample holder described in Fig. 3 was attached about 20 mm beneath the reflection head with an 18 mm focal length lens, therefore the beam waist at the tablet surface is about 2 mm. A bespoke immersion cell setup (Fig. 4) was then employed to investigate liquid transport through the coating layer and the tablet core. This setup was adapted from the one described before [39]. In this setup, the sample holder was immersed into the cell filled with 100 cm^3 room temperature water. The terahertz acquisition commenced before the sample holder was immersed in the deionised water, ensuring the entire water transport process was captured. Data were acquired continuously at 1 Hz rate. The acquisition was terminated when no stable reflection peak was evident any longer in the time-domain waveforms. The sample holder was then lifted from the solution and washed with warm tap water. The immersion cell was also replaced with fresh water before the following experiment. The experiment at each tablet porosity and film coating formulation was repeated twice.

The standard TPI signal deconvolution process and analysis were performed using MATLAB (MathWorks, Natick, MA, USA) [28,39]. The raw data file exported from the Terapulse 4000 spectrometer was converted to the dotTHz format before the deconvolution process [40]. The raw signal T was treated as a convolution between the sample signal S and instrument signal I and the noise (or baseline B) from the background air. By taking a fast Fourier transform, the sample signal can be considered in terms of the raw, reference, and baseline signals. A double-

Table 1
Details of the pure MCC tablets before and after the film coating process. The values quoted in the table are the average values of the film coated MCC tablets with the 95% confidence interval of the averages.

Target	Coating	Actual porosity	M_{before}/mg	M_{after}/mg	H_{before}/mm	H_{after}/mm
10%	PVA	10.1% ± 0.1%	289.6 ± 0.2	306.8 ± 1.0	1.546 ± 0.001	1.649 ± 0.008
	HPMC	10.1% ± 0.1%	288.9. ± 0.8	313.8 ± 0.5	1.543 ± 0.005	1.655 ± 0.005
15%	PVA	15.4% ± 0.1%	275.3 ± 0.2	293.2 ± 0.3	1.559 ± 0.001	1.658 ± 0.005
	HPMC	15.3% ± 0.2%	275.4 ± 0.6	299.0 ± 0.6	1.558 ± 0.001	1.659 ± 0.003
20%	PVA	20.5% ± 0.1%	257.2 ± 0.2	275.0 ± 0.9	1.547 ± 0.001	1.644 ± 0.005
	HPMC	20.4% ± 0.1%	257.4 ± 0.7	280.4 ± 2.7	1.548 ± 0.004	1.645 ± 0.010

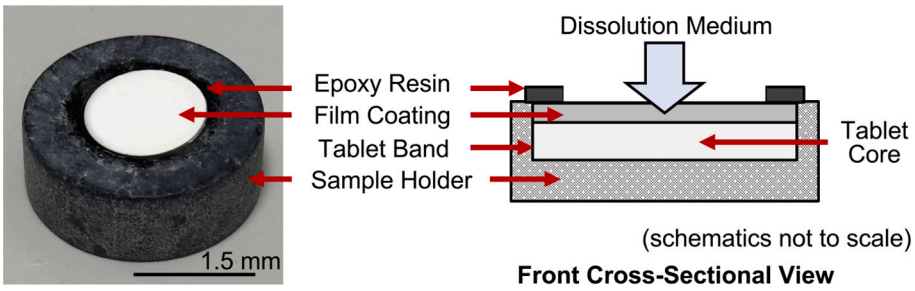

Fig. 3. The 3-D printed sample holder. A film-coated tablet is placed in the aperture. The band of the tablet is then sealed using epoxy resin so that the dissolution medium can only enter *via* the film-coated surface.

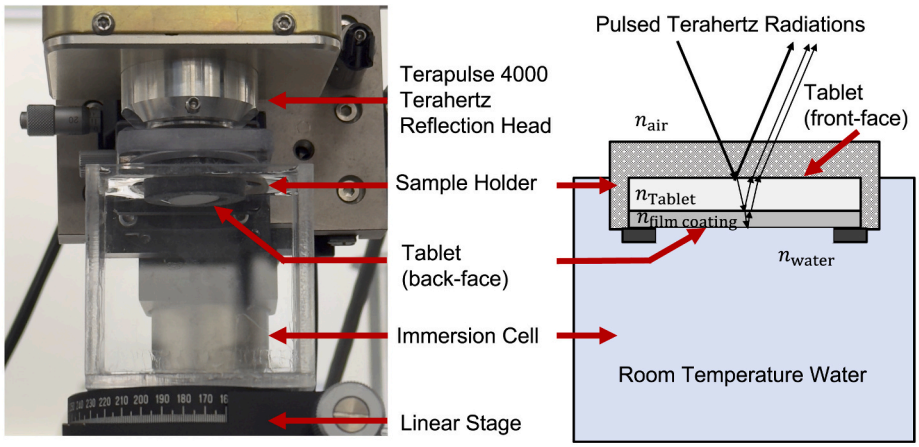

Fig. 4. The immersion cell design for the terahertz pulsed imaging measurements. The sample holder described in Fig. 3 is mounted on a stage holding the terahertz reflection head and immersed into the room temperature water held in an about 100 cm^3 customised plastic cuvette. Water only hydrates the tablet from the film-coated side since the uncoated band of the tablet is sealed with UV-hardened epoxy resin.

Gaussian band-pass filter was applied in the frequency domain to improve the waveform contrast and filter out the noise at high and low frequencies. As a final step, the Fourier synthesis transformed the sample signal back into the time domain for subsequent processing.

To visualise the time evolution of characteristic reflection peaks in the time-domain waveforms, each succeeding waveform was plotted above its preceding waveform with a vertical offset. This method generated the waterfall plot (Fig. 5(a)). The waterfall plot representation assisted the visual tracking of time-dependent features, *e.g.*, the water transport through tablets, by locating the peaks and the peak intensities on the plot. A two-phase process can be clearly identified in Fig. 5(a): the dissolution of the film coating and the water capillary penetration in the MCC core. The MATLAB-embedded "findpeak" function was utilised to track the characteristic reflection peaks on the waterfall plot. These peaks were extracted to quantify the tablet disintegration later in Section 3.

2.5. OCT measurement and data analysis

A Ganymede Series commercial spectral-domain preconfigured OCT system (Thorlabs Inc., Newton, New Jersey, USA) with 880 nm central wavelength was coupled to the flow cell described in Fig. 6(a) to scan the cross-sectional area of the film coating (OCT B-scans) on tablets. The sample holder was mounted with a test tablet in Fig. 3 and attached to the flow cell before the cell chamber was filled with room-temperature deionised water. The OCT requires the sample light path length to be equal to the reference light path length. The dissolution medium changes the optical path length of the light. Therefore, this must be compensated for by re-focussing the OCT beam on the film-coated surface of the tablet before the dissolution starts to capture the swelling behaviour from the beginning. The field-of-view of the B-scan area is approximately 1.5 mm and 8.2 mm along the thickness and radial direction of the tablet. The chamber was then emptied and dried, and the test tablet was replaced with the film-coated tablet of interest. The 2-D OCT B-scan commenced before filling water into the chamber using a peristaltic pump at 1.0 rpm that generates a flow rate of 2.9 mL min^{-1}. Images were acquired at 5-s intervals until 1500 s passed since the start of dissolution. MATLAB's "findpeak" function was used to track sudden changes in OCT intensity at the film-coated surface hydrated by the deionised water on OCT images (Fig. 6(b)). Thus, the extent of polymer swelling or dissolution during the tablet hydration process can be characterised if we calibrate the position of this surface at 0 s as zero point.

3. Results and discussion

3.1. Dissolution of immediate release film coating

The data extracted from TPI and OCT measurements (Fig. 5(b) and 7(a)) offer complementary information on the film coating dissolution process. Eq. (1) shows that the amplitude of the reflected terahertz pulse is proportional to the difference in the effective refractive indices n_{eff} between two media. Since water normally has the greatest n_{eff} value of the materials under investigation at terahertz frequencies, the water accumulation in the film coating during the hydration process leads to a noticeable rise in terahertz amplitude for about 150 s initially (Fig. 5(b), Phase 1). Quantitatively, we can uncover the amount of water accumulated in the film coating by analysing the increase in terahertz amplitude, assuming the rise in terahertz amplitude is proportional to the extent of coating hydration. The amplitude plot of the TPI signal also

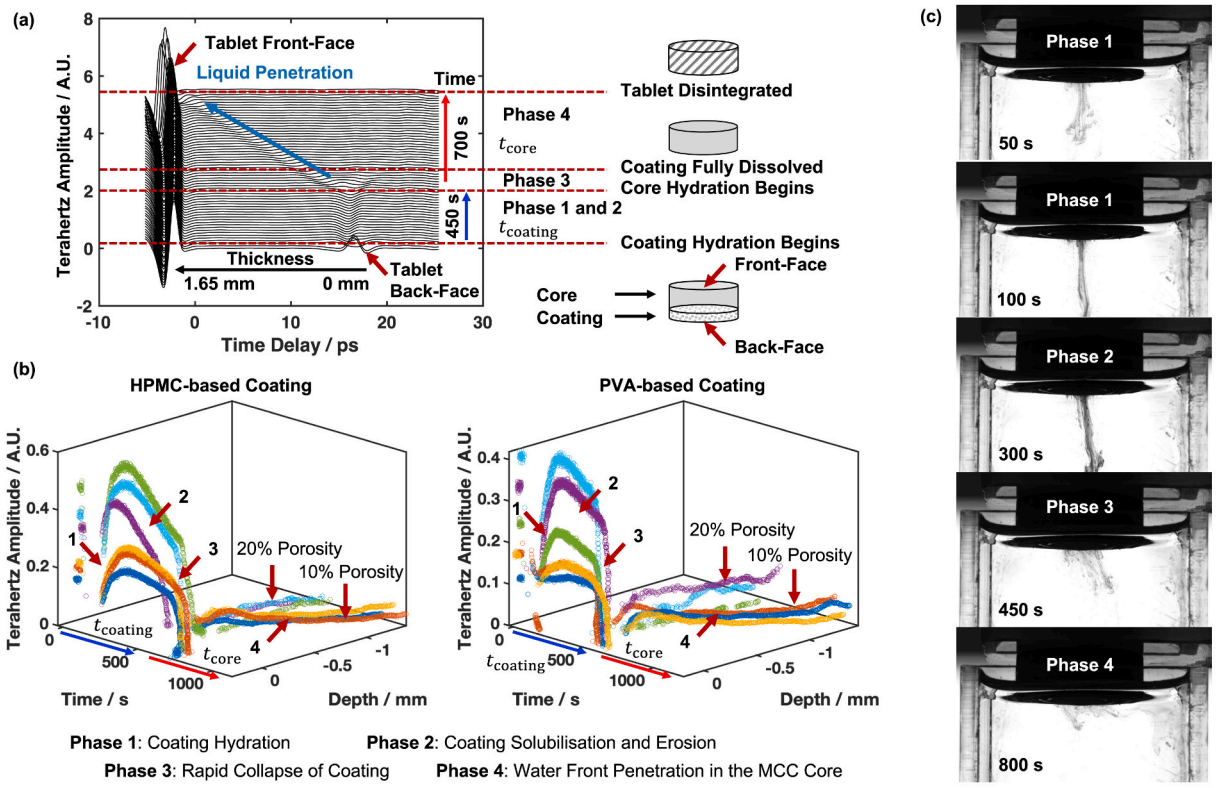

Fig. 5. The analysis of TPI results. (a) The waterfall plot showing the water transport process through a 10% porosity pure MCC tablet core with PVA-based film coating. The waveforms are stacked to describe the movement of the water front after the TPI measurement is commenced. (b) Changes of terahertz signal amplitude tracked from (a) as the water hydrates the film coating and penetrates through the 10% porosity MCC tablet core. Noticeable rise and fall in the signal amplitude can be found during the film coating dissolution process. In contrast, a gradual decline in signal amplitude is witnessed during the tablet core water transport process. The different lines represent repeats of measurement. Possible events during the hydration process are labelled in the figure. (c) Visual inspection on the different phases of disintegration. The dissolution process has already commenced in Phase 1. The steady solubilisation and erosion are seen in Phase 2. These phenomena can still be observed in Phase 3, when the film coating dissolution has almost finished, whereas almost no coating dissolution is witnessed in Phase 4 after the coating has fully dissolved.

provides direct access to the analysis of the film coating dissolution process. The processed terahertz amplitude is plotted on the z-axis in Fig. 5(b). We witness the gradual decline in the terahertz amplitude at around 300 s as the polymer in the film coating begins to slowly dissolve (Fig. 5(b), Phase 2). This is attributed to the distribution of water molecules in the coating polymer that creates a different phase, which will be discussed later in Section 3.3. This new phase has a lower n_{eff} than free water at terahertz frequencies due to the mixing with polymer molecules of lower refractive index and the disruption of the dense hydrogen bonding network of bulk water. The dissolution of film coating coating is a complex process, including hydration, solubilisation, erosion, and swelling, to name a few. The umbrella term "dissolution" was used to describe these processes in the previous publications [3,6]. The end of the dissolution of film coating is then characterised by the sharp fall of the terahertz amplitude (Fig. 5(b), Phase 3) to a level below 30% of the initial terahertz amplitude that was recorded prior to the film coating hydration process. Hence, the average film coating dissolution rate, $v_{coating}$, can then be calculated by dividing the coating thickness by the time taken for the terahertz amplitude to drop to this level (Table 2). We find values of $v_{coating}$ average at around 0.2 μm s^{-1}, which suggests a 100 μm thick film coating requires about 500 s to dissolve without agitation in room temperature water. Therefore, this measurement can be translated into about 150 s for a typical 30 μm thick immediate release film coating to dissolve, assuming a uniform polymer dissolution rate.

We characterise the swelling process of the polymer in the film coating of a separate set of samples using OCT (Fig. 7(a)). During the hydration process, an OCT A-scan along the thickness direction of the film-coated tablet enables a direct characterisation of the boundary between the coated surface and dissolution medium (Fig. 2A). We then sweep the OCT scan along the radial direction of the tablet to obtain OCT images (Fig. 6(b)), which allows us to resolve the changes along the B-scan line spatially (Fig. 2B). In addition to capturing the swelling process of the polymer, the OCT method further reveals that the weak points in the film coating are located in the region closer to the band of the tablet where the coating dissolution rate was fasted. The coating thickness in the previous study using X-ray computed tomography [3] was almost uniform. Thus, we speculate that additional stress is developed at the boundary with the epoxy resin near the band because of the inhomogeneous polymer swelling. In the OCT images, a "step change" is found near the epoxy resin reference site (Fig. 6(b)). This makes the polymer more permeable and can dissolve more rapidly. The non-uniform coating dissolution rate then suggests that the water front is less likely to be uniform and parallel to the diameter of the tablet as water hydrates the film coating.

The initial thickness increase of the coating layer in the first 150 s following hydration, shown in Fig. 7(b), is solely due to the swelling of the coating polymer after water diffuses into the porous matrix of the tablet core. The power law model (Eq. 2) was previously used to investigate the swelling kinetics as well [24,28], therefore, the process was repeated here to work out the swelling rate of PVA- and HPMC-based coating layer using the power law model. The modified Schott model (Eq. 4) was also utilised to study the one-dimensional polymer swelling process [41].

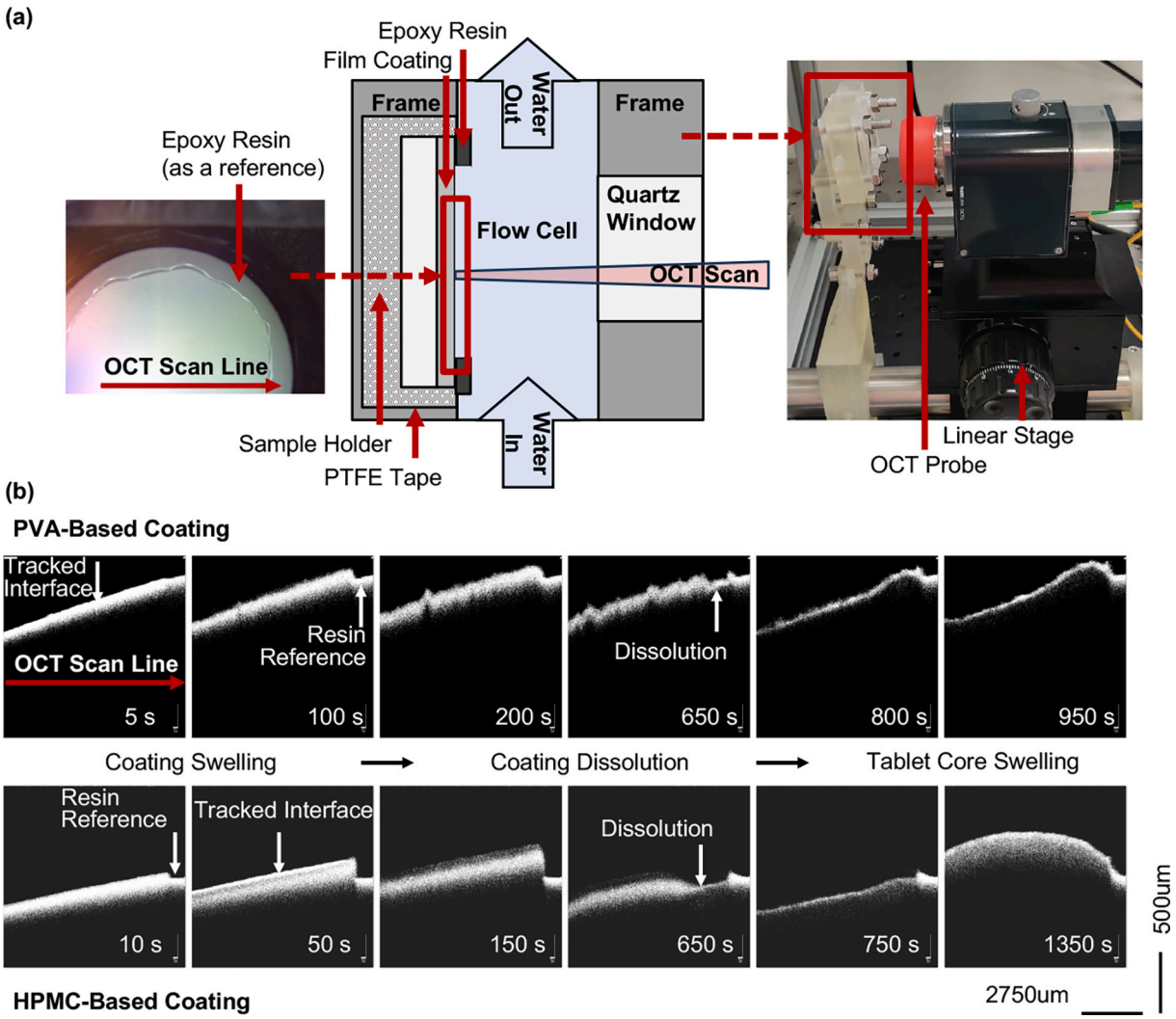

Fig. 6. The OCT experiment design and results. (a) The flow cell design for optical coherence tomography (OCT) experiments. A 3-D printed three-layer flow cell was employed with the OCT probe mounted on a horizontal linear stage to the right-hand side of this cell. Room-temperature water flows gradually through the central chamber of the cell that is sandwiched between two frames. The OCT scans were focussed on the film-coated surface of the tablet through the quartz window and the water (both are transparent to OCT operating frequencies). The sample holder in Fig. 3 holds the tablet. The OCT probe shown is currently in the "off" state. The protection lid needs to be removed before commencing measurements. (b) OCT images of the coated tablet cross-section along the scan line describing the PVA- and HPMC-based coating dissolution process and the subsequent MCC tablet core swelling process. The tablet core porosity is about 10%, and the coating thickness is about 100 μm. The "resin reference" is covered by the UV-hardened epoxy resin so that the coating at this point is free from hydration. The MATLAB algorithm tracks the interface changes at the middle point of the field of view (labelled).

$$\Delta\delta = \frac{t}{\alpha + \frac{1}{\delta_\infty - \delta_0} t} \tag{4}$$

where $\Delta\delta = \delta - \delta_0$ is the extent of swelling, α is the reciprocal of the initial swelling rate, δ_0 is the initial thickness of the polymer layer, and δ_∞ is the maximum possible thickness of the polymer layer. The Schott model is based on the second-order kinetics of liquid uptake in the swelling medium and thus provides more physical insights for modelling the swelling process [41].

The results summarised in Fig. 7(b) show that the HPMC-based film coating swells about four times faster on average than the PVA-based film coating. The modified Schott model also reveals that the initial swelling rate of HPMC-based coating is 4.46 times as fast as its PVA-based counterpart (Table 2). As HPMC has a more rigid polymer backbone than PVA, the HPMC polymer will exhibit reduced chain mobility and slower chain disentanglement during the film coating hydration. Therefore, the HPMC-based film coating shows a greater swelling rate. The modified Schott model predicts that both types of film coatings will exhibit similar theoretical extent of swelling at about 240 μm. However, the PVA based-coating is observed to swell to a much smaller maximum thickness (120 μm) than this theoretical value because of the film coating dissolution. The difference in power law model constants (k and m) in Table 2 denote that the PVA- and HPMC-based film coatings swell under different mechanisms. While the swelling kinetics of PVA-based coatings show zero-order kinetics, the HPMC-based counterpart undergoes a more thickness-dependent swelling process. Prior research has established that the swelling driving force stems from the difference in the chemical potential between water molecules and the dry particles [42]. The swelling rate also depends on the water diffusion coefficient in the particles and the (initial) size of particles [43]. Since PVA and HPMC are the major components in the film coating formulation, their ability to interact with water molecules will dominate the swelling kinetics of the film coating.

3.2. Water transport in the tablet core

The tablet core disintegration takes place following the film coating dissolution (Fig. 5(b), Phase 4) for MCC tablets. The water front

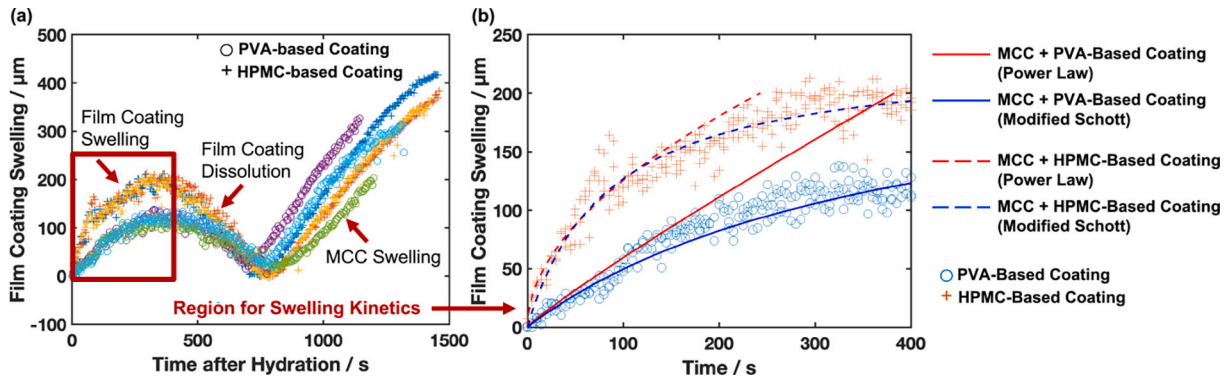

Fig. 7. (a) The swelling of the water-tablet interface tracked from the OCT images shown in Fig. 6(b) as water hydrates the film-coated MCC tablet. The metrics here clearly quantify the swelling and dissolution of the film coating and the swelling of the 10% porosity MCC tablet core. Datapoints with different colours represent repeats of measurement at the same porosity. (b) The swelling kinetics of PVA- and HPMC-based film coating following hydration. The red and blue curves are the best-fit curves for the polymer swelling kinetics using the power law model and modified Schott model, respectively. The initial film coating thickness is about 100 μm. The experimental results show that the PVA-based film coating is able to swell to a maximum of 120 μm while the swelling of the HPMC-based counterpart can reach about 200 μm. Only data from the first 150 s of polymer swelling are fitted in the models. The best-fit curves are extrapolated beyond 150 s to show the theoretical film coating swelling without dissolution. (For interpretation of the references to colour in this figure legend, the reader is referred to the web version of this article.)

Table 2
Summary of the film coating swelling models and the rate of film coating hydration. The swelling model is applied to the data for up to 150 s within which the coating swelling is the dominant process.

Type of coating	Power law model	Modified Schott model	Coating hydration $v_{coating}/\mu m\,s^{-1}$
PVA-based	$\Delta\delta = 0.810t^{0.898}$	$\Delta\delta = \frac{t}{1.61 + 0.00410t}$	0.230 ± 0.014
HPMC-based	$\Delta\delta = 12.6t^{0.505}$	$\Delta\delta = \frac{t}{0.361 + 0.00427t}$	0.195 ± 0.013

propagation in the tablet core can be effectively tracked from the depth-resolved features in the TPI waterfall plot. In contrast, the OCT images (Fig. 6(b)) reveal the core polymer (MCC) swelling process instead. One possible approach to quantify and compare the water front penetration rate is to compute the average core transport rate, v_{core}, by measuring the time it takes for water to penetrate to half of the thickness of the tablet core t_{core} (because the tablets are only film coated on one side, *c.f.* Table 4). Results are summarised in Table 3. Another approach is to investigate the kinetics of tablet core water penetration and swelling using the power law model. The metrics in Table 3 illustrate that the tablet core penetration rate and swelling rate are independent of the type of film coating once errors have been considered.

Noticeably, the water front penetration rates in the MCC tablet core after coating dissolution (Fig. 8) are much slower when comparing them with results obtained in previous studies of uncoated MCC tablets [24]. The uncoated 10% porosity MCC tablet becomes fully hydrated within about 15 s whereas the water penetration process following the coating dissolution takes more than 500 s for the entire tablet, and about 300 s to 400 s for the first half of the tablet. Similar results were reported in our previous TPI study on the dissolution of immediate-release film-coated tablets [6]. Meanwhile, the swelling of uncoated MCC cores alone is reported at a much faster rate (about 16 μm s^{-1}) in a study using 10% porosity uncoated MCC tablets [24]. After the film coating had dissolved, we found that the swelling rate for MCC had declined by a factor of greater than 20. We noticed from the OCT images that the film coating closer to the band of the tablet dissolves faster than the coating near the centre of the tablet (Fig. 6(b)). As a result, water wicks into the tablet core from the region near the tablet band, while the centre of the tablet core is still covered by a more or less intact film coating. Hence, the available area for initial water wicking will be much smaller than is the case for uncoated tablets, and the water penetration slows down.

Table 3
Summary of the power law liquid penetration kinetics, the liquid penetration time through the first 50% tablet core thickness, *i.e.*, the full penetration time t_{hyd}, and the average rate of liquid front penetration v_{core} in the MCC tablets.

MCC porosity	Coating base	Kinetics model/μm	t_{hyd} /s	v_{core} /μm s^{-1}
10%	PVA	$y = 3.29t^{0.913}$	824 ± 164	1.71 ± 0.29
	HPMC	$y = 4.16t^{0.921}$	826 ± 94	2.44 ± 0.23
15%	PVA	$y = 19.0t^{0.711}$	685 ± 121	2.99 ± 1.61
	HPMC	$y = 12.5t^{0.786}$	772 ± 109	3.26 ± 2.06
20%	PVA	$y = 57.0t^{0.669}$	525 ± 74	9.82 ± 3.26
	HPMC	$y = 37.2t^{0.727}$	552 ± 200	8.54 ± 3.14

The fitted *m* constant in the power law is correlated with the liquid mass transport mechanism. Suppose the water penetration behaviour, which is relatively incompressible, in the porous matrix of the tablet core can be modelled as the capillary rise taking place in the parallel cylinders. In that case, the value of this constant is close to 0.5. The *m* value will deviate from 0.5 if there are changes in the porous matrix or the water ingress behaviour. We previously found the *m* value to remain around 0.5 for uncoated MCC tablets at higher porosities but increase to about 0.75 for tablets at lower porosities [24]. This inverse porosity dependence happens because the swelling of MCC changes the structure of the porous matrix, and the MCC has a greater opportunity to swell in lower porosity tablets where the water front penetration is slow. Here, since the water penetration is much slower in film-coated tablets, the swelling of MCC in the tablet core is no longer negligible. With *m* constants close to unity in those film-coated tablets with 10% MCC porosity, significant MCC swelling may narrow the capillaries of the porous matrix. The water penetration is more likely to be driven by the concentration gradient of water between the inside and the outside of the matrix following the MCC swelling that leads to zero-order water transport kinetics [24]. Furthermore, the swelling is observed to have strong inverse porosity dependence. The MCC core swells less in tablets at 20% porosity, with its *m* value remaining around 0.75. This shows there is considerable swelling at higher porosity as well. Still, the extent of swelling is smaller than in the case at 10% porosity so that the *m* value deviates less from 0.5 at higher porosity.

The formulation of the tablet core and the temperature of the dissolution medium can influence the water transport in the core and, hence, the disintegration of the film-coated tablet. If soluble APIs or excipients are formulated in the core, they will dissolve, creating

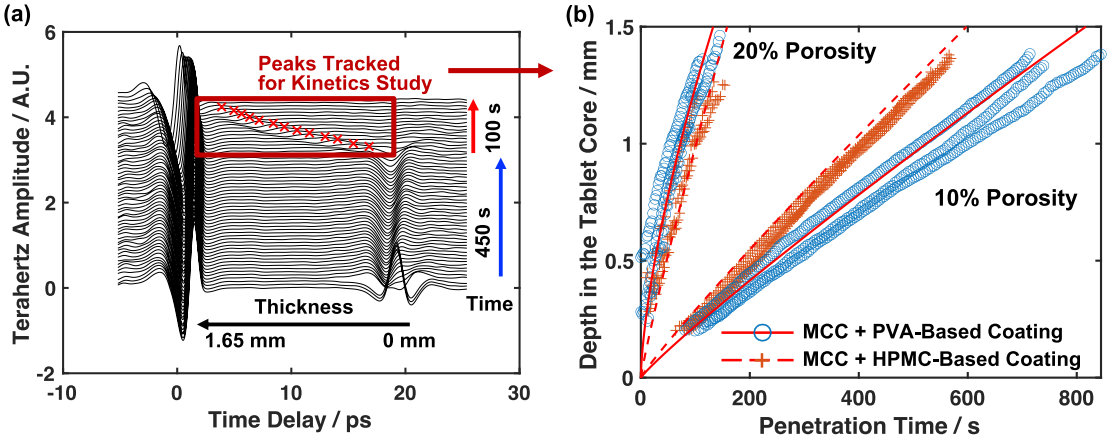

Fig. 8. (a) An example of the peak tracking process in the waterfall plot for the kinetics study. The waterfall plot shows the TPI results of a 20% MCC tablet film coated with the PVA-based coating formulation. (b) The water penetration kinetics in 10% and 20% porosity MCC cores following the film coating dissolution. The initial MCC core thickness is about 1.5 mm. The red curves are the best-fit lines for the kinetics using the TPI experiment data. The time required to hydrate the first half of the tablet is representative of water ingress from both faces of the tablet. (For interpretation of the references to colour in this figure legend, the reader is referred to the web version of this article.)

additional pore space in the core. As a result, the water mass transport mechanism will no doubt further deviate from the simple capillary rise mechanism. Meanwhile, the extent of overall bulk core swelling will vary depending on the composition of the core. For example, suppose a disintegrant is included in the tablet core. In that case, the disintegrant particles will swell considerably and rapidly, resulting in mechanical strain that leads to crack formation and rapid erosion of the tablet core. In the case of a film-coated tablet, this strain release may cause the film coating to rupture, further accelerating the coating dissolution and completing API release much earlier. Although the tensile strength of a typical film coating layer is about an order of magnitude higher than that of the tablet core, which prevents strain release from the core in dry conditions, the hydration of the film coating layer results in its tensile strength becoming comparable to the tablet core. An increase of water temperature from about 21°C to 37°C, *i.e.* the body temperature, will further accelerate the mass transport. The time required to dissolve the film-coating polymer will therefore decrease. At the same time, the water front will penetrate the MCC core much faster, which is likely to increase the disintegration or dissolution rate of the film-coated tablet.

3.3. The barrier effect

When the film coating is fully hydrated, and the water molecules reach the boundary between the film coating and the tablet core, the water front cannot penetrate the porous matrix of the core immediately, as the film coating layer restricts the propagation of the water molecules. This is experimentally evident from the TPI results (Fig. 5(a)), where the advancing water front becomes stationary upon reaching the coating-core interface. This barrier effect has been observed and discussed previously [3]. In contrast, the water transport into the tablet core starts immediately when an uncoated tablet surface is exposed to water [8,24,28].

The polymer dissolution process follows a complex mechanism [44]. When dry and below its glass transition temperature, the polymer is in a glassy state, and hence, the macromolecules remain quite rigid. Adding water molecules during hydration triggers the polymer dynamics to transition to a rubbery phase, imparting molecular mobility that facilitates the polymer solubilisation and subsequent dissolution. The process was first summarised in detail by Ueberreiter [9], who explored the depth-resolved complexity of the microstructure of polymers below the surface in contact with the dissolution medium. Ueberreiter described the process as a stratification of the polymer dynamics into four different regimes with increasing mobility and water content from the dry core (pure polymer) to the pure solvent: infiltration layer, solid swollen layer, gel layer and liquid layer. This model aligns broadly with the experimental observations from TPI and OCT. There are no sharp interfaces between each domain that separate clear layers of different polymer dynamics. The transition between the domains is gradual, which is in line with the mechanism articulated by Ueberreiter.

In contrast to the porous matrix of the uncoated tablet, there are no pores available in a cured film coating for capillary transport of water directly into the coating layer (Fig. 9(a)). However, apart from the voids between the molecules due to the free volume of the polymer phase, the film coating formulation contains a considerable fraction of a readily water-soluble polymer. Water molecules can enter the film coating layer *via* channels that form between the PVA or HMPC domains in the respective coating structures. Water quickly fills these channels and interacts *via* hydrogen bonding with the polymers in the film coating. The water front penetration is relatively fast due to the channels that form in the film coating, the volume of which was previously occupied by the soluble polymer (Fig. 9(b)). Water molecules penetrate the free volume of the polymer domains, resulting in an increase in macromolecular mobility and the polymer dynamics to transition to the rubbery state. With increasing water concentration, gel formation commences before the coating polymer is fully solubilised. As a result the film coating layer is swelling from its initial thickness L, to a swollen thickness S. The hydrated film coating contains a growing liquid-rich rubbery layer, R and a receding solid-rich glassy layer (S-R, Fig. 9(c)).

The OCT swelling data shows that the MCC core swells before the film coating has fully dissolved (Fig. 7(a)). This observation suggests the porous matrix is accessible to water molecules, and some diffusional water transport process can take place through the film coating (Fig. 9(d)). In contrast to the uncoated tablets, which do not have these surface layers, the apparent water permeability to the MCC core is significantly reduced. This means that the supply of water molecules to the MCC core is limited until the film coating has dissolved. Moreover, the soluble content needs to leave the tablet core *via* diffusion through the gel barrier of the coating layer (Fig. 9(d)). However, since MCC is insoluble in water, in this specific experiment, only negligible dissolution of the MCC core is detected in the TPI waterfall plots (Fig. 5(a)). If MCC is replaced with other soluble components, the components can dissolve in water and diffuse out of the core through the hydrated film coating.

The concept of so-called competitive hydration [45,46] emphasises the thermodynamic penalty for water molecules at the coating-core boundary that creates a barrier to penetrate into the porous matrix of the MCC core. The chemical potential difference that is driving the

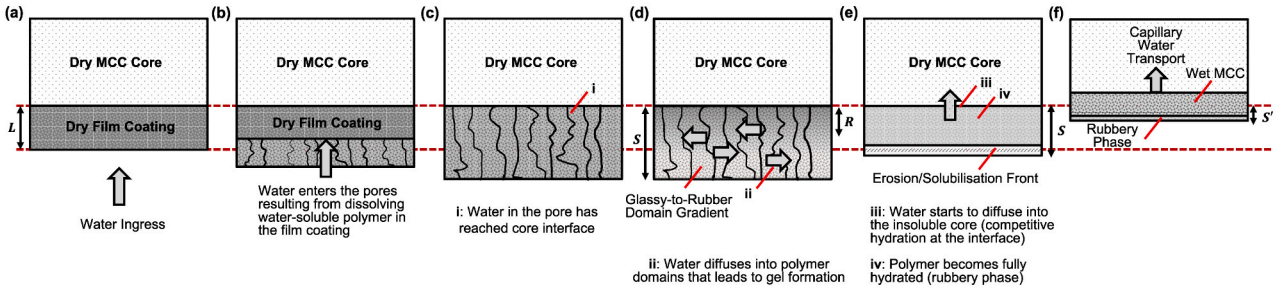

Fig. 9. The film coating polymer dissolution process. (a) The film coating layer (of thickness *L*) of the tablet remains in the dry state before the water ingress. (b) Water predominantly enters the pores, resulting in the successive dissolution of the water-soluble polymer within the film coating layer. In parallel, slower diffusion of water into the free volume of the polymer domains starts. (c) Water that is propagating along the pore has reached the interface with the tablet core. (d) Water continues to diffuse into the polymer domains surrounding the channels, resulting in further gel formation. A gradient of glassy-to-rubbery domain has developed in the hydrated film coating: *S*, the rubbery-to-solvent interface; *R*, the glassy-to-rubbery interface. (e) The film coating polymer becomes fully hydrated, and water starts to diffuse into the insoluble core. Competitive hydration at the interface between the coating and core restricts the capillary water transport into the porous matrix in the MCC core. (f) Following the film coating dissolution, capillary water transport begins in the MCC core, which is captured by TPI. The diffusional water transport has resulted in some MCC swelling, as evidenced by the OCT swelling data.

diffusion process across the film thickness competes with the chemical potential gradient due to the entropy and enthalpy changes of subsequent hydration in the tablet core at the interface between the coating and tablet core after water molecules arrive at the coating-core boundary (Fig. 9(e)). The number of water molecules bonded to the polar groups of the material, the hydration number, determines a material's ability to attract water molecules [47]. A hydration shell around the polymer can be formed after the water molecules hydrogen bond to the polar groups. Since the polymers in the film coating have higher polar group fractions along its polymer chain than MCCs in the tablet core, the majority of water molecules hydrogen bond to the film coating layer even if the water molecules reside at the boundary between the film coating and the tablet core after the film coating becomes saturated with water. This results in a temporary water transport barrier. The PVA-

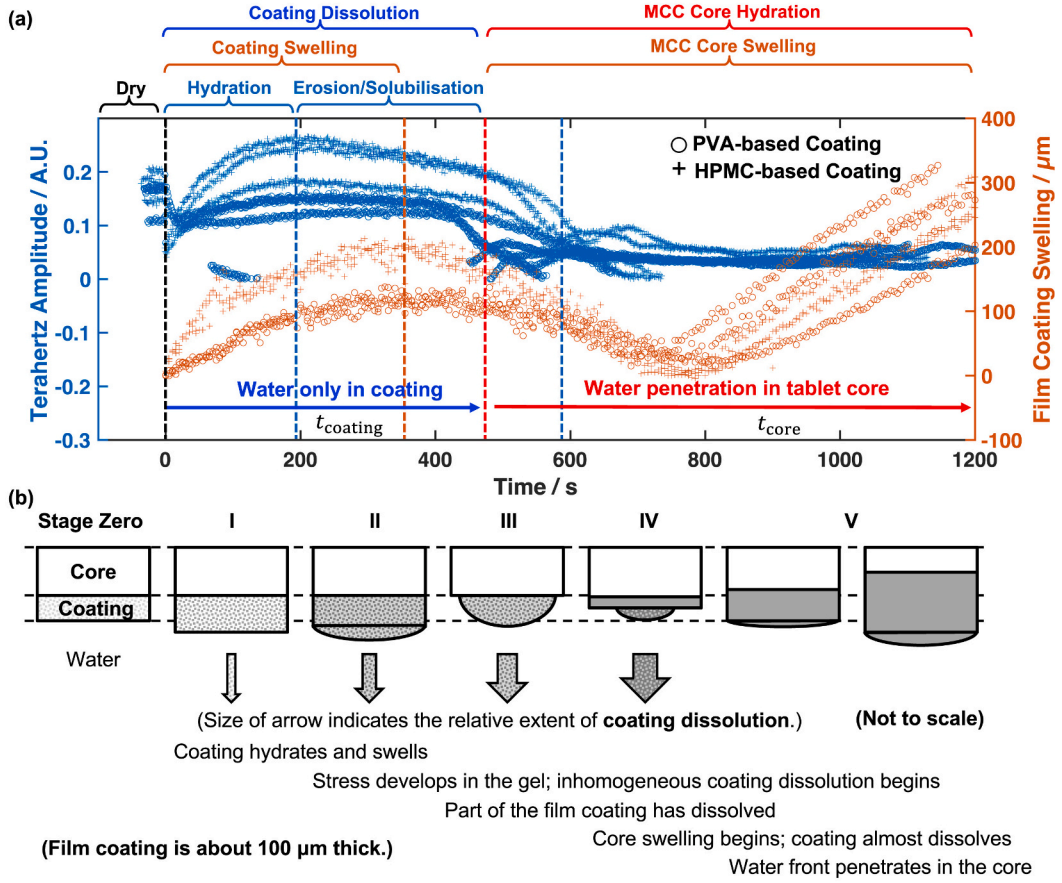

Fig. 10. The disintegration mechanism for a film-coated swelling tablet core summarised from the observations extracted from TPI and OCT data. (a) The upper and lower sections of the plot exhibit the changes in TPI amplitude and the film coating swelling, respectively. TPI is helpful for extracting the hydration process, while OCT is more sensitive to the swelling process. Both methods can be used to investigate the film coating dissolution process. (b) Schematics showing the possible events during the disintegration process based on the data presented in (a). The tablet core remains dry until Stage III, when the inhomogeneous coating dissolution rate provides the dissolution medium with shortcuts to reach the tablet core. The rate of tablet core swelling depends on the porosity of the core.

based and HPMC-based film coatings will exhibit different water permeability due to the different hydration numbers of PVA and HPMC [47,48] and the different hydration shells formed around the polymer. However, MCC has poorer solubility than PVA or HPMC in water [49]. Fig. 5(c) clearly shows that the majority of dissolution takes place as the film coating, which contains PVA or HPMC, dissolves. Little MCC dissolution can be observed after the complete film dissolution. Moreover, the hydrophilicity/hydrophobicity of the components in the tablet core and the film coating will determine the surface wetting properties. The water droplet is reported with a smaller wetting angle on the air-PVA interface (44° ±6°) [50] than on the air-HPMC interface (58° to 86°, depending on the HPMC grade) [51]. The water contact angle at the MCC-air interface is reported from about 57° to 71° [49]. This means that the film coating will be more readily to be wetted during the tablet disintegration process. Hence, only a limited number of water molecules can diffuse into the MCC core that is not sufficient to cause capillary water transport in the porous matrix until the film coating surface layer has become thin enough (Fig. 9(f)).

3.4. Proposed film coated tablet disintegration mechanism

The associated metrics from the results of TPI and OCT in Fig. 5(b) and 7(a) can be inspected in parallel to extract information on the processes of coating dissolution and the tablet core hydration. The metrics provide complementary illustrations of the behaviours of hydration, swelling, solubilisation, and erosion of the film coating. In addition to the hydration kinetics of the MCC core, the swelling kinetics of the MCC core can also be seen in Fig. 10(a). Therefore, the disintegration process of a film-coated tablet can be deduced by inspecting the associated metrics in Fig. 10(a). Hereby, we propose the film-coated tablet disintegration mechanism as summarised in Fig. 10(b).

The surface wetting process of the coating layer is assigned as **Stage Zero**. The surface tension at the coated surface needs to be overcome before water can wick into the film coating. As a result of water wicking, the coating layer begins swelling and dissolving. Then, **Stage I** describes the coating layer hydration and swelling process. The increase in the terahertz signal amplitude shows that water starts to accumulate in the coating layer rapidly. As more water hydrates the coating polymer, the coating layer swells sharply. However, the swelling rate gradually decreases because the coating polymer becomes saturated with bulk or free water molecules. The coating layer continues to dissolve, yet the dissolution rate is much smaller than the swelling rate. Therefore, the overall thickness of the coating layer slowly increases. Water molecules can diffuse in the polymer layer and form hydrogen bonds with the coating polymer, disrupting the intermolecular forces holding the coating film together. Therefore, the amplitude of the terahertz signal declines slowly in **Stage II**. This process leads to a glassy-to-rubbery gradient in the polymer so that a gel layer gradually develops in the coating. The extent of coating swelling rate almost reaches the maximum. The gel layer will protects the tablet core from capillary water ingress and only the outmost part of the film coating can slowly erode or solubilise. However, materials are allowed to diffuse through the hydrated polymer. Water can diffuse into the tablet core that triggers the slow core swelling. As the gel is exposed to the dissolution medium for a significantly long period, the inhomogeneity can be introduced in the film coating and the medium will find shortcuts to reach the tablet core (**Stage III**). This process can lead to further core swelling, which will push the gel layer apart and introduce further permeability and reduce the polymer density of the gel layer. Consequently, the quick dissolution of the gel layer results in a sudden drop in the terahertz signal (**Stage IV**). Finally, following the collapse of the gel layer, capillary water transport begins in the tablet core and induces rapid MCC swelling in **Stage V**. Noticeably, Stages I-IV, which account for the film-coating dissolution, takes up more than half of the total time for the water to hydrate the entire film-coated MCC tablet (Table 4). If the MCC core is more porous (for example, at 20% porosity), Table 4 shows that the film coating dissolution becomes the rate-determining process for the disintegration of the coated MCC tablet. The polymer dissolution have been discussed in detail in Section 3.3.

Table 4
Comparison between the time spent to dissolve the film coating in room temperature water $t_{coating}$ and the time spent for the water front to penetrate half of the MCC core following the film coating dissolution t_{core}. Data assume the tablet has 100 μm-thick layer of film coating on 1.5 mm-thick MCC tablet and use the calculated $v_{coating}$ and v_{core} from Table 2 and Table 3.

MCC porosity	Coating base	t_{core}/s	$t_{coating}$/s	$t_{coating}/(t_{coating} + t_{core})$
10%	PVA	439 ± 77	452 ± 69	0.508 ± 0.031
	HPMC	308 ± 28	524 ± 79	0.630 ± 0.015
15%	PVA	260 ± 160	484 ± 63	0.654 ± 0.114
	HPMC	241 ± 159	587 ± 60	0.712 ± 0.122
20%	PVA	77 ± 25	418 ± 22	0.844 ± 0.038
	HPMC	86 ± 31	506 ± 99	0.855 ± 0.044

4. Conclusions

The disintegration process of film-coated immediate-release tablets was studied using TPI and OCT in room-temperature water. Either PVA-based or HPMC-based coating formulations were film-coated on pure MCC tablets produced by direct compression. Results from this model system suggest a film coating layer of about 100 μm thickness takes about 500 s to dissolve under the experiment conditions fully. The MCC core porosity plays little role in determining the rate of film coating dissolution. The film coating hydrates and swells before dissolution takes place. The dissolution of the film coating involves the transform of coating polymer from the glassy to rubbery phase so that water molecules will be able to diffuse in the said polymer to promote coating erosion or solubilisation. However, the capillary water transport does not take place until the rubbery phase polymer becomes thin enough and no longer restricts the water molecules because of competitive hydration. The MCC core itself begins swelling when water diffuses through the film coating, which results in the swelling force pushing the film coating apart to create further paths for water to enter the MCC core. The power law model was used to study the kinetics of the film coating swelling and water front penetration in the MCC core based on the results from TPI and OCT. As the power law model suggests that the water penetration in the MCC core is less likely to resemble as the capillary rise, the core is believed to swell as well, and therefore, this reduces the rate of water front penetration in the porous matrix of the MCC core. The said rate is also much lower than the rate in uncoated counterparts because the barrier effect from the film coating extends the MCC swelling that narrows down the channels for water penetration. The swelling kinetics of the film coating and the tablet core depend on their ability to interact with water molecules. The phenomena observed during the disintegration of the film-coated MCC tablet were summarised into a potential disintegration mechanism of film-coated tablets without tablet core erosion and agitation in the dissolution medium. This mechanism can be further utilised to understand film-coated tablets with modified release characteristics.

Future work will be required to study the disintegration process of film-coated tablets using water at body temperature as the dissolution medium. This will help to understand the temperature dependence of the gelling process of coating polymers. It will also be interesting to use simulated gastric fluids to study the effects of pH on the coating dissolution. Although initially limited to pure MCC tablets, further investigations may explore the impact of more complex tablet core formulations. For example, the core can be formulated step-wise by extending it from a pure excipient to a drug and another commonly used excipient, such as lactose. On the film-coating side, tablets with different coating thicknesses can be employed to corroborate if the exact disintegration mechanism would apply to all these film-coated tablets. The investigation will be extended to sustained release tablets as well.

Equipment permitting, the research can include simultaneous or parallel TPI and OCT characterisation.

CRediT authorship contribution statement

Mingrui Ma: Writing – original draft, Validation, Software, Methodology, Funding acquisition, Formal analysis. **Marwa Nassar:** Writing – review & editing, Methodology, Investigation. **Jason Teckoe:** Writing – review & editing, Resources, Project administration. **Daniel Markl:** Writing – review & editing, Resources, Methodology, Conceptualization. **J. Axel Zeitler:** Writing – original draft, Supervision, Resources, Project administration, Methodology, Funding acquisition, Conceptualization.

Declaration of competing interest

The authors declare the following financial interests/personal relationships that may be considered as potential competing interests: M. Ma reports that financial support was provided by CSC. J.A. Zeitler reports equipment, drugs, or supplies was provided by Colorcon Ltd.

Data availability

Data will be made available on request.

Acknowledgements

M.M. would like to acknowledge funding by CSC Cambridge International Scholarship from the Cambridge Commonwealth, European & International Trust, UK in partnership with the China Scholarship Council. D.P. and D.M. would like to acknowledge funding from the EPSRC (EP/W003295/1; EP/S02168X/1) to support the OCT work in this study.

Appendix A. The compaction simulator

Fig. A.11 shows a typical compaction profile to make an MCC tablet at about 10% porosity, including information on both the punch positions and the compaction force.

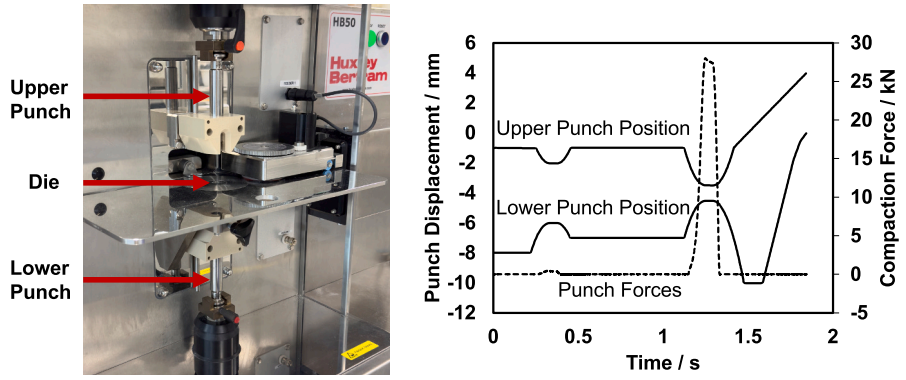

Fig. A.11. The compaction simulator and an exemplar compaction profile for compacting MCC powders into round 13 mm flat-faced tablets. The MCC powder is filled into the die before the lower and the upper punch close to exert forces on the free-flow powder to compact it into cylindric-shaped tablets. The porosities of the resultant tablets depend on the powder fill weight in the die, the compaction force exerted by the punches, as well as the type of powder used.

Appendix B. Additional waterfall plots

Two exemplar water plots are attached in Fig. B.12 to illustrate the disintegration process of MCC tablets film coated with HPMC-based coating formulations capture by TPI. The film coating dissolution is similar at both 10% and 20% porosities, whereas the said film coating takes longer to dissolve than the PVA-based film coating.

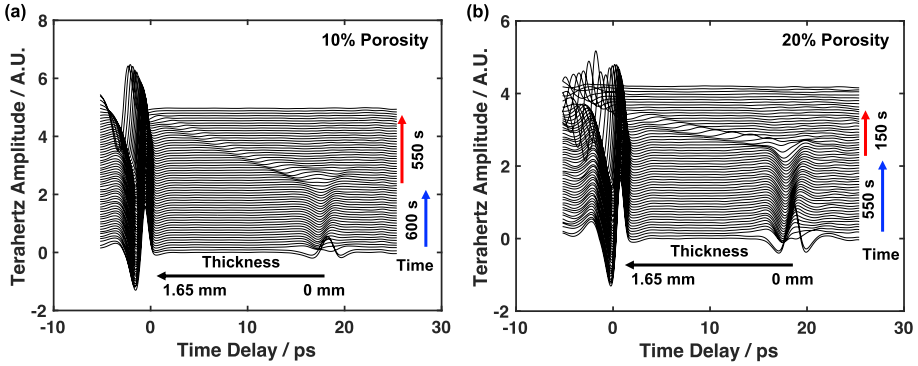

Fig. B.12. Additional waterfall plots showing the water transport process through (a) a 10% porosity and (b) a 20% porosity pure MCC tablet core with HPMC based film coating. The waveforms are stacked to describes the movement of the water front after the TPI measurement is commenced.

References

[1] K.J. Bittorf, T. Sanghvi, J.P. Katstra, Design of solid dosage formulations, in: D.J. am Ende (Ed.), Chemical Engineering in the Pharmaceutical Industry Ch. 36, John Wiley & Sons, Inc, 2010, pp. 673–702, https://doi.org/10.1002/9780470882221.ch36.

[2] G. Göran Frenning, Chapter 31: Tablets and compaction, in: K.M.G. Taylor, M. E. Aulton (Eds.), Aulton's Pharmaceutics: The Design and Manufacture of Medicines Ch. 31, Elsevier, 2022, pp. 719–776.

[3] R. Dong, M. Nassar, B. Friend, J. Teckoe, J.A. Zeitler, Studying the dissolution of immediate release film coating using terahertz pulsed imaging, Int. J. Pharm. (2023) 122456, https://doi.org/10.1016/j.ijpharm.2022.122456.

[4] L. Ho, R. Müller, M. Römer, K. Gordon, J. Heinämäki, P. Kleinebudde, M. Pepper, T. Rades, Y. Shen, C. Strachan, P. Taday, J. Zeitler, Analysis of sustained-release tablet film coats using terahertz pulsed imaging, J. Control. Release 119 (2007) 253–261, https://doi.org/10.1016/j.jconrel.2007.03.011.

[5] L. Ho, R. Müller, K.C. Gordon, P. Kleinebudde, M. Pepper, R. Thomas, Y. Shen, P. F. Taday, J.A. Zeitler, Applications of terahertz pulsed imaging to sustained-release tablet film coating quality assessment and dissolution performance, J. Control. Release 127 (1) (2008) 79–87, https://doi.org/10.1016/j.jconrel.2008.01.002.

[6] R. Dong, J.C. DiNunzio, B.P. Regler, W. Wasylaschuk, A. Socia, J.A. Zeitler, Insights into the control of drug release from complex immediate release formulations, Pharmaceutics 13 (2021) 933, https://doi.org/10.3390/pharmaceutics13070933.

[7] R. Dong, J.A. Zeitler, Visualising liquid transport through coated pharmaceutical tablets using terahertz pulsed imaging, Int. J. Pharm. (2022) 121703, https://doi.org/10.1016/j.ijpharm.2022.121703.

[8] S. Yassin, K. Su, H. Lin, L.F. Gladden, J.A. Zeitler, Diffusion and swelling measurements in pharmaceutical powder compacts using terahertz pulsed imaging, J. Pharm. Sci. 104 (2015) 1658–1667, https://doi.org/10.1002/jps.24376.

[9] K. Ueberreiter, The solution process, in: J. Crank, G.S. Park (Eds.), Diffusion in Polymers, Academic Press, New York, NY, 1968, pp. 219–257.

[10] H. Nogami, T. Nagai, E. Fukuoka, T. Sonobe, Disintegration of the aspirin tablets containing potato starch and microcrystalline cellulose in various concentrations, Chem. Pharm. Bull. 17 (7) (1969) 1450–1455, https://doi.org/10.1248/cpb.17.1450.

[11] P. Catellani, P. Predella, A. Bellotti, P. Colombo, Tablet water uptake and disintegration force measurements, Int. J. Pharm. 51 (1989) 63–66, https://doi.org/10.1016/0378-5173(89)90075-6.

[12] J. Quodbach, P. Kleinebudde, Systematic classification of tablet disintegrants by water uptake and force development kinetics, J. Pharm. Pharmacol. 66 (2014) 1429–1438, https://doi.org/10.1111/jphp.12276.

[13] J. Tomas, M. Schöngut, O. Dammer, J. Beránek, A. Zadražil, F. Štěpánek, Probing the early stages of tablet disintegration by stress relaxation measurement, Eur. J. Pharm. Sci. 124 (2018) 145–152, https://doi.org/10.1016/j.ejps.2018.08.029.

[14] P.M. Desai, C.V. Liew, P.W.S. Heng, Understanding disintegrant action by visualization, J. Pharm. Sci. 101 (2012) 2155–2164, https://doi.org/10.1002/jps.23119.

[15] Q. Zhang, L.F. Gladden, P. Avalle, J.A. Zeitler, M.D. Mantle, Terahertz pulsed imaging and magnetic resonance imaging as tools to probe formulation stability, Pharmaceutics 5 (2013) 591–608, https://doi.org/10.3390/pharmaceutics5040591.

[16] J. Quodbach, A. Moussavi, R. Tammer, J. Frahm, P. Kleinebudde, Tablet disintegration studied by high-resolution real-time magnetic resonance imaging, J. Pharm. Sci. 103 (2014) 249–255, https://doi.org/10.1002/jps.23789.

[17] H. Lin, Y. Dong, Y. Shen, J.A. Zeitler, Quantifying pharmaceutical film coating with optical coherence tomography and terahertz pulsed imaging: an evaluation, J. Pharm. Sci. 104 (2015) 3377–3385, https://doi.org/10.1002/jps.24535.

[18] M.H. Gaunø, T. Vilhelmsen, C.C. Larsen, J.P. Boetker, J. Wittendorff, J. Rantanen, J. Østergaard, Real-time in vitro dissolution of 5-aminosalicylic acid from single ethyl cellulose coated extrudates studied by uv imaging, J. Pharm. Biomed. Anal. 83 (2013) 49–56, https://doi.org/10.1016/j.jpba.2013.04.028.

[19] J. Østergaard, J. Lenke, S.S. Jensen, Y. Sun, F. Ye, Uv imaging for in vitro dissolution and release studies: initial experiences, Dissolution Technol. (2014) 27–38, https://doi.org/10.14227/DT210414P27.

[20] A. Axelsson, M. Marucci, The use of holographic interferometry and electron speckle pattern interferometry for diffusion measurement in biochemical and pharmaceutical engineering applications, Opt. Lasers Eng. 46 (2008) 865–876, https://doi.org/10.1016/j.optlaseng.2008.03.017.

[21] N. O'Mahoney, J.J. Keating, S. McSweeney, S. Hill, S. Lawrence, D. Fitzpatrick, The sound of tablets during coating erosion, disintegration, deaggregation and dissolution, Int. J. Pharm. 580 (2020) 119216, https://doi.org/10.1016/j.ijpharm.2020.119216.

[22] J. Lenz, F. Fuest, J.H. Finke, H. Bunjes, A. Kwade, M. Juhnke, Tablet disintegration and dispersion under in vivo-like hydrodynamic conditions, Pharmaceutics 14 (1) (2022) 208, https://doi.org/10.3390/pharmaceutics14010208.

[23] A.J. Fitzgerald, B.E. Cole, P.F. Taday, Nondestructive analysis of tablet coating thicknesses using terahertz pulsed imaging, J. Pharm. Sci. 94 (1) (2005) 177–183, https://doi.org/10.1002/jps.20225.

[24] S. Yassin, D.J. Goodwin, A. Anderson, J. Sibik, D.I. Wilson, L.F. Gladden, J. A. Zeitler, The disintegration process in microcrystalline cellulose based tablets, part 1: influence of temperature, porosity and superdisintegrants, J. Pharm. Sci. 104 (2015) 3440–3450, https://doi.org/10.1002/jps.24544.

[25] P. Bawuah, D. Markl, D. Farrell, M. Evans, A. Portieri, A. Anderson, D. Goodwin, R. Lucas, J.A. Zeitler, Terahertz-based porosity measurement of pharmaceutical tablets: a tutorial, J. Infrared Millim. Terahertz Waves 41 (2020) 450–469, https://doi.org/10.1007/s10762-019-00659-0.

[26] R.K. May, M.J. Evans, S. Zhong, I. Warr, L.F. Gladden, Y. Shen, J.A. Zeitler, Terahertz in-line sensor for direct coating thickness measurement of individual tablets during film coating in real-time, J. Pharm. Sci. 100 (4) (2011) 1535–1544, https://doi.org/10.1002/jps.22359.

[27] D. Markl, P. Wang, C. Ridgway, A.-P. Karttunen, P. Bawuah, J. Ketolainen, P. Gane, K.-E. Peiponen, J.A. Zeitler, Resolving the rapid water absorption of porous functionalised calcium carbonate powder compacts by terahertz pulsed imaging, Chem. Eng. Res. Des. 132 (2018) 1082–1090, https://doi.org/10.1016/j.cherd.2017.12.048.

[28] M. Al-Sharabi, D. Markl, T. Mudley, P. Bawuah, A.-P. Karttunen, C. Ridgway, P. Gane, J. Ketolainen, K.-E. Peiponen, R. Thomas, J.A. Zeitler, Simultaneous investigation of the liquid transport and swelling performance during tablet disintegration, Int. J. Pharm. 584 (2020) 119380, https://doi.org/10.1016/j.ijpharm.2020.119380.

[29] A. Leitenstorfer, A.S. Moskalenko, T. Kampfrath, J. Kono, E. Castro-Camus, K. Peng, N. Qureshi, D. Turchinovich, K. Tanaka, A.G. Markelz, M. Havenith, C. Hough, H.J. Joyce, W.J. Padilla, B. Zhou, K.-Y. Kim, X.-C. Zhang, P.U. Jepsen, S. Dhillon, M. Vitiello, E. Linfield, A.G. Davies, M.C. Hoffmann, R. Lewis, M. Tonouchi, P. Klarskov, T.S. Seifert, Y.A. Gerasimenko, D. Mihailovic, R. Huber, J.L. Boland, O. Mitrofanov, P. Dean, B.N. Ellison, P.G. Huggard, S.P. Rea, C. Walker, D.T. Leisawitz, J.R. Gao, C. Li, Q. Chen, G. Valšis, V.P. Wallace, E. P.-M, X. Shang, J. Hesler, N. Ridler, C.C. Renaud, I. Kallfass, T. Nagatsuma, J.A. Zeitler, D. Arnone, M.B. Johnston, J. Cunningham, The 2023 terahertz science and technology roadmap, J. Phys. D Appl. Phys. 56 (2023) 223001, https://doi.org/10.1088/1361-6463/acbe4c.

[30] D. Markl, G. Hannesschläger, S. Sacher, M. Leitner, J.G. Khinast, Optical coherence tomography as a novel tool for in-line monitoring of a pharmaceutical film-coating process, Eur. J. Pharm. Sci. 55 (2014) 58–67, https://doi.org/10.1016/j.ejps.2014.01.011.

[31] E. Fink, S. Celikovic, J. Rehrl, S. Sacher, J.A.A. Urich, J. Khinast, Prediction of dissolution performance of uncoated solid oral dosage forms via optical coherence tomography, Eur. J. Pharm. Biopharm. 189 (2023) 281–290, https://doi.org/10.1016/j.ejpb.2023.07.003.

[32] D. Koller, G. Hannesschläger, M. Leitner, J. Khinast, Non-destructive analysis of tablet coatings with optical coherence tomography, Eur. J. Pharm. Sci. 44 (2011) 142–148, https://doi.org/10.1016/j.ejps.2011.06.017.

[33] M. Wolfgang, A. Kern, S. Deng, S. Stranzinger, M. Liu, W. Drexlerb, R. Leitgebb, R. Haindl, Ultra-high-resolution optical coherence tomography for the investigation of thin multilayered pharmaceutical coatings, Int. J. Pharm. 643 (2023) 123096, https://doi.org/10.1016/j.ijpharm.2023.123096.

[34] M. Wolfgang, S. Stranzingera, J.G. Khinast, Ascertain a minimum coating thickness for acid protection of enteric coatings by means of optical coherence tomography, Int. J. Pharm. 618 (2022) 121680, https://doi.org/10.1016/j.ijpharm.2022.121680.

[35] S. Zhong, Y.-C. Shen, L. Ho, R.K. May, J.A. Zeitler, M. Evans, P.F. Taday, M. Pepper, T. Rades, K.C. Gordon, R. Müller, P. Kleinebudde, Non-destructive quantification of pharmaceutical tablet coatings using terahertz pulsed imaging and optical coherence tomography, Opt. Lasers Eng. 49 (2011) 361–365, https://doi.org/10.1016/j.optlaseng.2010.11.003.

[36] H. Lin, Y. Dong, Y. Shen, J.A. Zeitler, Quantifying pharmaceutical film coating with optical coherence tomography and terahertz pulsed imaging: an evaluation, J. Pharm. Sci. 104 (10) (2015) 3377–3385, https://doi.org/10.1002/jps.24535.

[37] C. Sun, True density of microcrystalline cellulose, J. Pharm. Sci. 94 (10) (2005) 2132–2134, https://doi.org/10.1002/jps.20459.

[38] M. Haaser, K. Naelapää, K.C. Gordon, M. Pepper, J. Rantanen, C.J. Strachan, P. F. Taday, J.A. Zeitler, T. Rades, Evaluating the effect of coating equipment on tablet film quality using terahertz pulsed imaging, Eur. J. Pharm. Biopharm. 85 (2013) 1095–1102, https://doi.org/10.1016/j.ejpb.2013.03.019.

[39] J. Lee, D.J. Goodwin, R.M. Dhenge, J. Nassar, G. Bano, J.A. Zeitler, Enhanced in-situ liquid transport investigation setup for pharmaceutical tablet disintegration analysis using terahertz radiation, Int. J. Pharm. 635 (2023) 122726, https://doi.org/10.1016/j.ijpharm.2023.122726.

[40] J. Lee, C.K. Leung, M. Ma, J. Ward-Berry, S. Santitewagun, J.A. Zeitler, The dotTHz project: a standard data format for terahertz time-domain data, J. Infrared. Millim. TerahertzWaves. 44 (2023) 795–813, https://doi.org/10.1007/s10762-023-00947-w.

[41] D. Markl, S. Yassin, D.I. Wilson, D.J. Goodwin, A. Anderson, J.A. Zeitler, Mathematical modelling of liquid transport in swelling pharmaceutical immediate release tablets, Int. J. Pharm. 526 (2017) 1–10, https://doi.org/10.1016/j.ijpharm.2017.04.015.

[42] J.M.R.J. Huyghe, J.D. Janssen, Quadriphasic mechanics of swelling incompressible porous media, Int. J. Eng. Sci. 35 (1997) 793–802, https://doi.org/10.1016/S0020-7225(96)00119-X.

[43] T. Sweijen, B. Chareyre, S. Hassanizadeh, N. Karadimitriou, Grain-scale modelling of swelling granular materials; application to super absorbent polymers, Powder Technol. (2017), https://doi.org/10.1016/j.powtec.2017.06.015.

[44] B.A. Miller-Chou, J.L. Koenig, A review of polymer dissolution, Prog. Polym. Sci. 28 (8) (2003) 1223–1270, https://doi.org/10.1016/s0079-6700(03)00045-5.

[45] C. Ajith, A.P. Deshpande, S. Varughese, Proton conductivity in crosslinked hydrophilic ionic polymer system: competitive hydration, crosslink heterogeneity, and ineffective domains, J. Polym. Sci. B 54 (2016) 1087–1101, https://doi.org/10.1002/polb.24012.

[46] N. Ekmekciyan, T. Tuglu, F. El-Saleh, C. Muehlenfeld, E. Stoyanov, J. Quodbach, Competing for water: a new approach to understand disintegrant t performance, Int. J. Pharm. 548 (2018) 491–499, https://doi.org/10.1016/j.ijpharm.2018.07.025.

[47] Y. Satokawa, T. Shikata, Hydration structure and dynamic behavior of poly(vinyl alcohol)s inaqueous solution, Macromolecules 41 (2008) 2908–2913, https://doi.org/10.1021/ma702793t.
[48] K. Arai, T. Shikata, Hydration/dehydration behavior of cellulose ethers in aqueoussolution, Macromolecules 50 (2017) 5920–5928, https://doi.org/10.1021/acs.macromol.7b00848.
[49] M.V. Hammesa, A.H. Englertb, C.P.Z. Noreñac, N.S.M. Cardozoa, Effect of water activity and gaseous phase relative humidity on microcrystalline cellulose water contact angle measured by the washburn technique, Colloids Surf. A Physicochem. Eng. Asp. 500 (2016) 118–126, https://doi.org/10.1016/j.colsurfa.2016.04.018.
[50] R. Jayasekara, I. Harding, I. Bowater, G. Christie, G. Lonergan, Preparation, surface modification and characterisation of solution cast starch pva blended films, Polym. Test. 23 (2004) 17–27, https://doi.org/10.1016/S0142-9418(03)00049-7.
[51] P. Kraisit, M. Luangtana-Anan, N. Sarisuta, Effect of various types of hydroxypropyl methylcellulose (hpmc) films on surface free energy and contact angle, Adv. Mater. Res. 1060 (2015) 107–110, https://doi.org/10.4028/www.scientific.net/AMR.1060.107.